10^{th} *International Conference on* HYDROELASTICITY IN MARINE TECHNOLOGY
Trondheim, Norway, June16$^{\mathrm{th}}$*-18*$^{\mathrm{th}}$*, 2026*

Inverse Wave Force Estimation Using Frequency- and Time-Domain Hydroelastic Models

Van Zijl, C.[1,*] Jovanova, J.[1], and Grammatikopoulos, A.[1]

[1] Department of Maritime & Transport Technology, Delft University of Technology, The Netherlands

Abstract. Accurate knowledge of wave-induced loads is essential for the safe and efficient design and operation of offshore structures, yet direct measurement of hydrodynamic forces remains challenging. This study investigates whether wave excitation forces can be estimated from measured structural responses by treating the structure as a distributed force sensor. A hydroelastic state-space model incorporating frequency-dependent added mass and radiation damping, obtained through rational approximation of radiation forces, is employed. A joint input–state Kalman filter is used to estimate both dynamic states and unknown excitation forces from noisy acceleration measurements. Its performance is evaluated against frequency-domain inverse methods based on least-squares inversion of acceleration frequency response functions, including a Tikhonov-regularised formulation to address ill-conditioning. Results show that accurate force reconstruction is primarily achieved within frequency ranges where the forward operator is well conditioned, particularly near modal resonances and for lower-order modes. While Tikhonov regularisation yields the lowest estimator variance, it introduces bias and underestimates force energy for higher-order modes. The time-domain Kalman filter provides a more balanced trade-off between variance reduction and bias through implicit regularisation introduced by system dynamics. The results demonstrate that regularisation improves estimator stability but may suppress physically relevant force content when applied excessively.

Key words: *Wave load estimation; inverse problems; Tikhonov regularization; Kalman filtering*

1. Introduction

Accurate knowledge of wave-induced loads enables engineers to design marine structures that can withstand the harsh ocean environment while optimising performance and operational efficiency. In the shipping and offshore industries, reliable estimates of wave forces support safe and efficient route planning, fuel optimisation, and structural health monitoring [1, 2]. Despite their importance, wave excitation forces are difficult or impossible to measure directly on large floating structures, motivating the use of inverse methods in which forces are inferred from measured structural responses.

Inverse force estimation relies on a forward model that relates external excitation to measured responses. In marine applications, this relationship is provided by hydroelastic models that couple structural dynamics with hydrodynamic loading. In the frequency domain, the forward model is commonly expressed through frequency response functions that incorporate frequency-dependent added-mass and radiation-damping effects [3]. In the time domain, these same hydrodynamic effects appear as radiation memory terms, typically represented through convolution kernels or equivalent state-space formulations [4]. Both representations describe the same underlying physics, but lead naturally to different inverse estimation approaches.

A fundamental challenge in inverse wave load estimation is the low-frequency nature of wave excitation acting on large floating structures. In the present context, "low-frequency" refers to first-order

*Correspondence to: c.m.vanzijl@tudelft.nl

wave excitation in the typical ocean-wave range (approximately 0.05–0.15 Hz, corresponding to wave periods of 7–20 s), which is substantially below the first wet natural frequencies of large ship structures (typically of order 1 Hz). In this regime, hydroelastic transfer operators are often ill-conditioned, leading to significant amplification of measurement noise in inverse solutions [5]. This effect is especially pronounced for higher-order modes and can limit the reliability of frequency-domain least-squares inversion. Time-domain formulations introduce implicit regularisation through their state-space representation and noise modelling, which may mitigate low-frequency variance amplification, but at the cost of increased dependence on the assumed model structure.

The aim of this paper is to examine frequency- and time-domain inverse wave force estimation methods within a consistent hydroelastic modelling framework. The focus is on a controlled comparison of commonly used inverse formulations applied to the same linear hydroelastic model, wave excitation, and measurement conditions. The frequency-domain approach is considered in least-squares and Tikhonov-regularised form. The regularisation parameter is selected using the L-curve criterion, yielding a global regularisation level that is subsequently scaled with frequency according to the magnitude of the forward operator singular values. The time-domain approach employs a joint input–state Kalman filter, in which regularisation arises implicitly through the system dynamics and noise modelling.

The remainder of the paper is organised as follows. Section 2 introduces the hydroelastic forward model and inverse formulations. Section 3 describes the numerical model and simulation setup. Section 4 presents the results, and Section 5 summarises the main findings.

2. Theory

This section introduces the hydroelastic forward model used for inverse wave load estimation and formulates the inverse problem in both the frequency and time domains. A linear hydroelastic model is adopted, allowing a frequency-domain representation based on transfer operators and a time-domain state-space formulation that includes radiation memory effects through a rational approximation. Superscript $(\cdot)^{(m)}$ denotes modal quantities.

2.1. Hydroelastic model

The hydroelastic system is represented in a truncated modal basis containing rigid-body and flexible structural modes. The modal basis matrix $\Phi \in \mathbb{R}^{n \times n_m}$ is constructed from the dry structural eigenvalue problem

$$\left(K_s - \omega_r^2 M_s\right) \phi_r = 0, \tag{1}$$

where M_s and K_s denote the dry structural mass and stiffness matrices, respectively. Using the modal coordinates $\underline{Y}^{(m)} \in \mathbb{R}^{n_m}$, the coupled hydroelastic equation of motion in the frequency domain becomes

$$\Big(- \omega^2 \big(M + M_h(\omega)\big) + i\omega\big(C + C_h(\omega)\big) + \big(K + K_h\big)\Big)\underline{Y}^{(m)}(\omega) = \underline{F}^{(m)}(\omega), \tag{2}$$

Here, M, C, and K denote the reduced structural mass, damping, and stiffness matrices in modal coordinates. The structural damping matrix C is assumed diagonal and constructed from prescribed modal damping ratios. Furthermore, $M_h(\omega)$ and $C_h(\omega)$ are the frequency-dependent added-mass and radiation-damping matrices and K_h is the hydrostatic restoring matrix.

2.2. Frequency-domain formulation

Define the modal hydroelastic frequency response function (FRF) as:

$$H^{(m)}(\omega) = (-\omega^2\big(M + M_h(\omega)\big) + i\omega\big(C + C_h(\omega)\big) + \big(K + K_h\big))^{-1}, \tag{3}$$

For acceleration measurements at selected physical locations, the measured response is

$$\underline{Y}(\omega) = -\omega^2 \, S\Phi \, H^{(m)}(\omega) \, \underline{F}^{(m)}(\omega) \;\triangleq\; \mathcal{H}(\omega) \, \underline{F}^{(m)}(\omega), \tag{4}$$

where S maps structural degrees of freedom to sensor locations. The operator $\mathcal{H}(\omega)$ therefore constitutes the forward model for inverse force estimation.

2.3. Time-domain formulation

For implementation of the time-domain joint input–state Kalman filter introduced later, the hydroelastic model is expressed in state-space form [4]. The use of a state-space realization for radiation-memory effects in combination with Kalman-filter-based force estimation follows the approach of [6]. The present work applies this framework to a hydroelastic system; the relevant equations are therefore summarized here for completeness.

2.3.1. Radiation memory and hydrodynamic state-space model

The time-domain equation of motion corresponding to Eq. (2) is:

$$(M + M_\infty)\ddot{\underline{y}}^{(m)}(t) + C\dot{\underline{y}}^{(m)}(t) + (K + K_h)\underline{y}^{(m)}(t) + \int_0^t K_r(t-\tau)\dot{\underline{y}}^{(m)}(\tau)\,\mathrm{d}\tau = \underline{f}^{(m)}(t), \tag{5}$$

where M_∞ is the infinite-frequency added mass. Define the radiation impedance

$$Z(\omega) \triangleq C_h(\omega) + i\omega\big(M_h(\omega) - M_\infty\big). \tag{6}$$

To avoid explicit evaluation of the radiation-memory convolution in Eq. (5), the radiation impedance is approximated by a finite-dimensional state-space realization. Using vector fitting, $Z(s)$ with $s = i\omega$ is approximated as

$$Z(s) \approx C_r(sI - A_r)^{-1}B_r, \tag{7}$$

where A_r, B_r, and C_r are realization matrices whose order is determined by the number of retained poles in the fit.This yields the hydrodynamic radiation subsystem

$$\dot{\underline{x}}_r^{(m)}(t) = A_r\,\underline{x}_r^{(m)}(t) + B_r\,\dot{\underline{y}}^{(m)}(t), \tag{8}$$

$$\underline{f}_{\text{rad}}^{(m)}(t) = C_r\,\underline{x}_r^{(m)}(t). \tag{9}$$

which replaces the convolution term with a finite-dimensional dynamical system suitable for time-domain state estimation and Kalman filtering.

2.3.2. Augmented hydroelastic state-space model

Combining the structural modal dynamics with the radiation subsystem yields a finite-dimensional state-space representation suitable for time-domain inverse estimation and Kalman filtering. Defining the effective inertia matrix $M_{\text{eff}} = M + M_\infty$ the modal acceleration equation becomes

$$\ddot{\underline{y}}^{(m)}(t) = -M_{\text{eff}}^{-1}(K + K_h)\underline{y}^{(m)}(t) - M_{\text{eff}}^{-1}C\dot{\underline{y}}^{(m)}(t) - M_{\text{eff}}^{-1}C_h\underline{x}_r^{(m)}(t) + M_{\text{eff}}^{-1}\,\underline{f}^{(m)}(t). \tag{10}$$

Introducing the augmented modal state vector

$$\underline{x}^{(m)}(t) = \begin{bmatrix} \underline{y}^{(m)}(t) \\ \dot{\underline{y}}^{(m)}(t) \\ \underline{x}_r^{(m)}(t) \end{bmatrix}. \tag{11}$$

The continuous-time augmented model is

$$\dot{\underline{x}}^{(m)}(t) = A\,\underline{x}^{(m)}(t) + B\,\underline{f}^{(m)}(t), \tag{12}$$

with

$$A = \begin{bmatrix} 0 & I & 0 \\ -M_{\text{eff}}^{-1}(K + K_h) & -M_{\text{eff}}^{-1}C & -M_{\text{eff}}^{-1}C_r \\ 0 & B_r & A_r \end{bmatrix}, \qquad B = \begin{bmatrix} 0 \\ M_{\text{eff}}^{-1} \\ 0 \end{bmatrix}. \tag{13}$$

2.4. Discrete-time model and acceleration output

For inverse estimation, (12) is discretised with sampling interval Δt,

$$\underline{x}_{n+1}^{(m)} = A_d\,\underline{x}_n^{(m)} + B_d\,\underline{f}_n^{(m)} + \underline{w}_n, \tag{14}$$

$$\underline{y}_n = C_d\,\underline{x}_n^{(m)} + D_d\,\underline{f}_n^{(m)} + \underline{v}_n, \tag{15}$$

where $\underline{w}_n \sim \mathcal{N}(0, Q)$ and $\underline{v}_n \sim \mathcal{N}(0, R)$. The measured output consists of accelerations at selected physical DOFs. Let Φ map modal to physical coordinates and S select sensor locations. The measurement matrices are

$$C_d = S\Phi\left[-M_{\text{eff}}^{-1}(K + K_h) \quad -M_{\text{eff}}^{-1}C \quad -M_{\text{eff}}^{-1}C_r\right], \tag{16}$$

$$D_d = S\Phi\,M_{\text{eff}}^{-1}. \tag{17}$$

2.5. Inverse force estimation

The objective is to estimate the unknown modal excitation force $\underline{f}^{(m)}$ from measured responses, given the hydroelastic forward model.

2.5.1. Frequency-domain least-squares inversion

In the frequency domain, the forward model reads

$$\underline{Y}(\omega_k) = \mathcal{H}(\omega_k)\,\underline{F}^{(m)}(\omega_k), \tag{18}$$

Assuming $\mathcal{H}_k$ has full column rank, the corresponding closed-form least-squares solution is

$$\underline{\widehat{F}}_k^{(m)} = \left(\mathcal{H}_k^{\mathrm{H}}\mathcal{H}_k\right)^{-1}\mathcal{H}_k^{\mathrm{H}}\,\underline{\tilde{Y}}_k \tag{19}$$

where $(\cdot)^{\mathrm{H}}$ denotes the Hermitian transpose.

2.5.2. Tikhonov-regularised frequency-domain inversion

In practice, the forward operator $\mathcal{H}_k$ may be ill-conditioned, particular at low frequencies. In this case, small singular values amplify measurement noise and lead to large estimator variance. To stabilise the inversion, Tikhonov regularisation is introduced. The regularised estimate has the following closed-form solution:

$$\underline{\widehat{F}}_k^{(m)} = \left(\mathcal{H}_k^{\mathrm{H}}\mathcal{H}_k + \lambda^2\mathbf{I}\right)^{-1}\mathcal{H}_k^{\mathrm{H}}\,\underline{\tilde{Y}}_k \tag{20}$$

where $\lambda > 0$ is the regularisation parameter controlling the trade-off between variance reduction and estimation bias. The global regularisation parameter is selected using the L-curve criterion [7].

2.5.3. Time-domain joint input–state Kalman filter

The discrete-time state-space model is used within the joint input–state estimation framework of Gillijns and De Moor [8], in which both the structural state and modal excitation forces are estimated sequentially from the measured acceleration response. The formulation exploits the direct feedthrough term in the measurement equation to obtain same-step force estimates from the measurement innovation while simultaneously updating the structural state.

3. Numerical model

A numerical study is conducted on an idealised floating beam to compare frequency- and time-domain inverse force estimation under controlled modelling and measurement noise.

3.1. Hydroelastic model

The structure is modelled as a uniform Euler–Bernoulli beam of length $L = 200$ m with circular cross-section radius $R = 10$ m and wall thickness $t = 1.7 \times 10^{-3}$ m. The Young's modulus is $E =$ 200 GPa. The material density is selected such that the beam floats at an approximate draft of $R/2$ and the first dry bending natural frequency is $f_1 \approx 0.2$ Hz. The first dry natural frequency is selected to be approximately consistent with the low-frequency global structural dynamics of large container ship structures, for which first natural frequencies are often of the order of 0.2 Hz. In real vessels, these low-frequency modes may typically correspond to torsional global modes, whereas the present simplified model exhibits only vertical bending responses. The beam model is therefore not intended to represent a specific vessel directly, but rather an idealised flexible floating structure with comparable low-frequency hydroelastic behaviour.

A finite-element model with 401 elements (402 nodes) is constructed. Modal truncation retains $n_m = 8$ dry modes, including rigid-body and flexible modes. A uniform modal damping ratio $\zeta = 0.02$ is assumed for all retained modes.

Frequency-dependent hydrodynamic coefficients are computed using the potential-flow boundary element solver CAPYTAINE [9]. The wetted surface is discretised using 7360 panels. For the retained modal basis, the added-mass and radiation-damping matrices $M_h(\omega)$ and $C_h(\omega)$ are obtained over the frequency range of interest. In addition, the modal wave-excitation force transfer functions (RAOs mapping wave elevation to modal forces) are also computed using CAPYTAINE. All hydrodynamic coefficients are computed for head-wave conditions (180° wave heading). Table 1 compares the dry and wet natural frequencies for a subset of modes of the coupled hydroelastic model, while the corresponding dry and wet mode shapes are shown in Fig. 1.

Table 1: Comparison of natural frequencies (in Hz) for dry and wet/coupled models. The flexible modes (Mode 3 and 4) are labeled using the convention XnVB, where X denotes the number of nodes in the mode shape and VB stands for vertical bending.

Mode name	**Dry model**	**Wet model**
Pitch	0.00	0.139
Heave	0.00	0.140
2nVB	0.229	0.228
3nVB	0.633	0.503

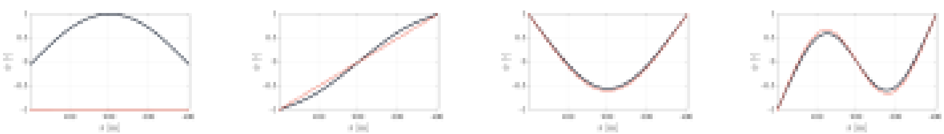

(a) Heave (b) Pitch (c) 2nVB (d) 3nVB

Figure 1: Mode shapes of four modes for the dry (solid line) and wet/coupled (dashed line) models.

The radiation impedance in Eq. (6) is approximated using vector fitting as described in Section 2.1.. The open-source MATLAB package `vectfitx` [10] is employed, using $N_p = 10$ poles per retained mode.

3.2. Numerical simulation procedure

Irregular wave excitation is modelled using a JONSWAP spectrum [11] with parameters $H_s = 3$ m, $T_p = 9$ s, and $\gamma = 3.3$. The spectrum is transformed to encounter frequency for head-wave conditions and forward speed of $U = 10$ m/s. A uniform random phase realisation is used to model random waves. Modal wave-excitation forces are then obtained from the hydrodynamic excitation-force RAOs computed using CAPYTAINE.

The corresponding noise-free structural response is generated using the hydroelastic forward model introduced in Section 2.1.. The resulting acceleration signals are sampled at 20 Hz over a duration of 2000 s and contaminated with additive zero-mean Gaussian noise with standard deviation 0.01 m/s^2.

For the frequency-domain inverse method, the sampled acceleration signals are transformed using an FFT with Hanning windowing prior to least-squares or Tikhonov inversion at each discrete frequency. For the time-domain approach, the measured acceleration time histories are used directly in the discrete-time hydroelastic state-space model together with the joint input–state Kalman filter described in Section 2.5..

4. Results

The results are presented in three parts. First, the accuracy of the rational approximation of the radiation impedance is assessed, as this directly determines the fidelity of the time-domain state-space model. Second, the variance characteristics of the frequency- and time-domain inverse force estimators are compared. Finally, the quality of the reconstructed force spectra is evaluated in terms of power spectral density and root-mean-square force levels.

4.1. Radiation impedance fitting accuracy

The quality of the rational approximation of the radiation impedance is quantified using the relative fitting error. The relative fitting error is defined as

$$\frac{\sum_{\omega}|Z(\omega) - \hat{Z}(\omega)|}{\sum_{\omega}|Z(\omega)|}. \tag{21}$$

Figure 2 shows the relative error for all entries of the 8×8 impedance matrix. The lowest errors are observed for the lower-order modes (modes 1–3), while significantly larger errors occur for the highest mode (mode 8). In general, diagonal terms exhibit smaller errors than off-diagonal terms, reflecting the fact that self-radiation effects are captured more accurately than modal coupling terms. Physically, entry (i, j) represents the radiation force in mode i induced by motion in mode j.

To illustrate the quality of individual fits, Figure 3 compares the real and imaginary parts of selected impedance terms. The $(2, 2)$ entry shows an good match between the true and fitted impedance over the frequency range of interest, with only minor amplitude deviations. In contrast, the $(8, 8)$ entry exhibits noticeably larger discrepancies, particularly in amplitude, consistent with the higher relative errors reported above. These results confirm that modelling errors increase with modal order and will therefore primarily affect force estimation in the higher modes.

4.2. Variance of force estimates

Figure 4 compares the variance of the estimated modal excitation forces for Modes 1–4 under measurement noise contamination. The variance quantifies how strongly the estimated forces fluctuate across different realizations of measurement noise and therefore provides a measure of estimator robustness to sensor noise. Lage values of variance indicate strong amplification of sensor noise through the inverse problem. The plotted quantity corresponds to the variance of the real part of the estimated modal forces and therefore has units of force squared (N^2).

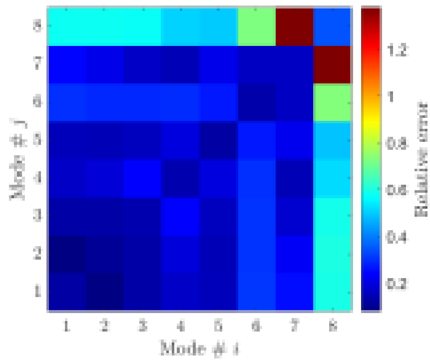

Figure 2: Relative fitting error of the rational approximation of the radiation impedance for all entries of the 8×8 modal impedance matrix. Each entry (i, j)corresponds to the radiation force in mode i induced by motion in mode j.

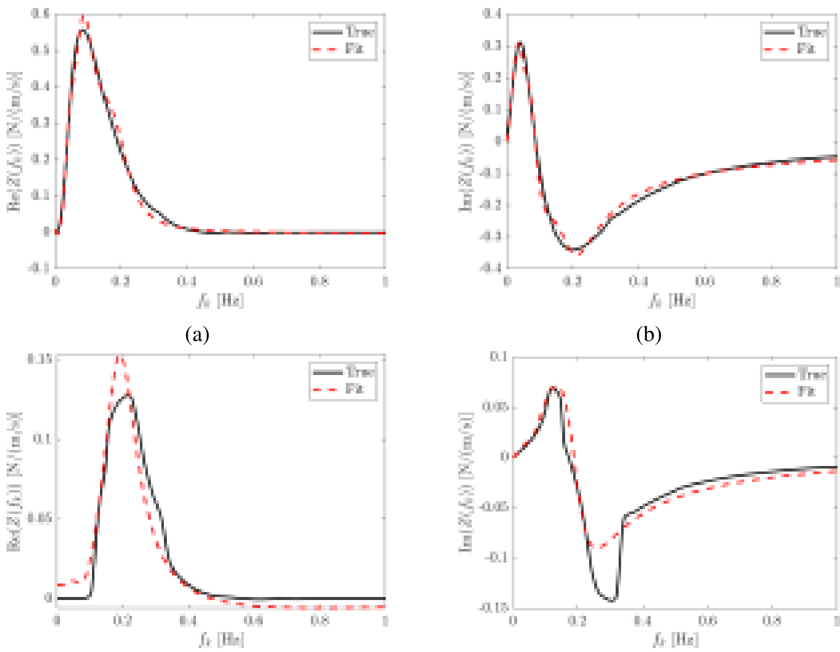

(a) (b)

(c) (d)

Figure 3: Comparison of the real and imaginary parts of the fitted and true radiation impedance for selected diagonal terms (2,2) and (8,8) of the modal impedance matrix over the frequency range of interest.

The large variation in variance across frequency highlights the strong frequency dependence of the inverse problem conditioning. Near the modal resonance frequencies, the measured accelerations are highly sensitive to the corresponding excitation forces, resulting in relatively low estimator variance.

Away from resonance, the differences between the estimators become pronounced. The unregularised LS solution exhibits strong variance amplification at low frequencies, particularly for higher-order modes, due to the ill-conditioning of the forward operator. The Kalman filter reduces this effect through implicit regularisation introduced by the state-space dynamics and noise modelling. The Tikhonov estimator produces the lowest variance overall by explicitly damping weakly observable singular directions of the inverse problem. However, this variance reduction reflects stronger regularisation rather than improved observability and must therefore be interpreted together with the bias characteristics discussed in the following section.

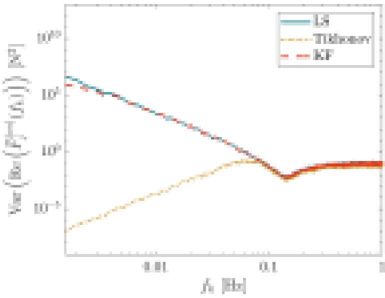

(a) Mode 1

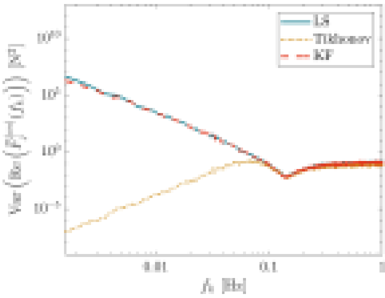

(b) Mode 2

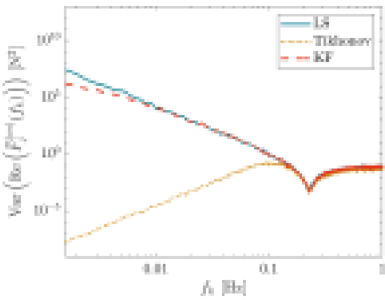

(c) Mode 3

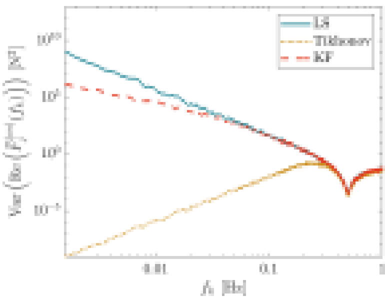

(d) Mode 4

Figure 4: Variance of the estimated modal wave-excitation forces for modes 1—4 as a function of frequency obtained using least-squares (LS), Tikhonov regularization, and the time-domain Kalman filter (KF).

4.3. Reconstruction of force spectra and RMS level

The quality of the reconstructed force spectra is examined by comparing the power spectral density (PSD) of the estimated forces with the true PSD. The area under the PSD is directly related to the root-mean-square (RMS) force contribution over a given frequency band. While the variance results in Section 4.1 indicate that the Tikhonov estimator provides the strongest stabilisation of the inverse problem, the PSD comparison reveals the associated increase in estimation bias.

For the LS estimator, the PSD is computed directly from the frequency-domain force estimate as $S_{F_jF_j}(\omega_k) = S_P\,|\hat{F}_j(\omega_k)|^2$, where S_P is a scaling factor ensuring consistency with the signal normalization. For the Kalman filter, the PSD is estimated from the time-domain force signal using Welch's method.

Figure 5 compares the reconstructed PSDs for Modes 1, 3, 5, and 7. For the lower-order modes, all estimators recover the true PSD reasonably well in the dominant excitation range around 0.1–0.3 Hz. Outside this range, the differences between the estimators become increasingly pronounced.

The LS estimator exhibits elevated PSD levels away from resonance due to strong amplification of measurement noise in ill-conditioned frequency regions. The Tikhonov estimator strongly suppresses these poorly observable components through explicit regularization. For the higher-order modes, particularly Modes 5 and 7, this suppression becomes so strong that the reconstructed force energy is several orders of magnitude lower than the true PSD over parts of the frequency range. This behaviour reflects the bias–variance tradeoff inherent to Tikhonov regularization: variance is substantially reduced, but at the cost of aggressively damping weakly observable force components toward zero.

The Kalman filter achieves a more balanced behaviour. Although its variance is generally higher than that of the Tikhonov estimator, the reconstructed PSD retains more physically relevant force content within the frequency range of interest. This suggests that the dynamical constraints imposed by the state-space model provide an effective form of implicit regularization without introducing the same level of bias suppression.

Although modelling errors in the fitted radiation dynamics increase with modal order, their effect on systematic bias is not clearly distinguishable from regularisation effects in the present results.

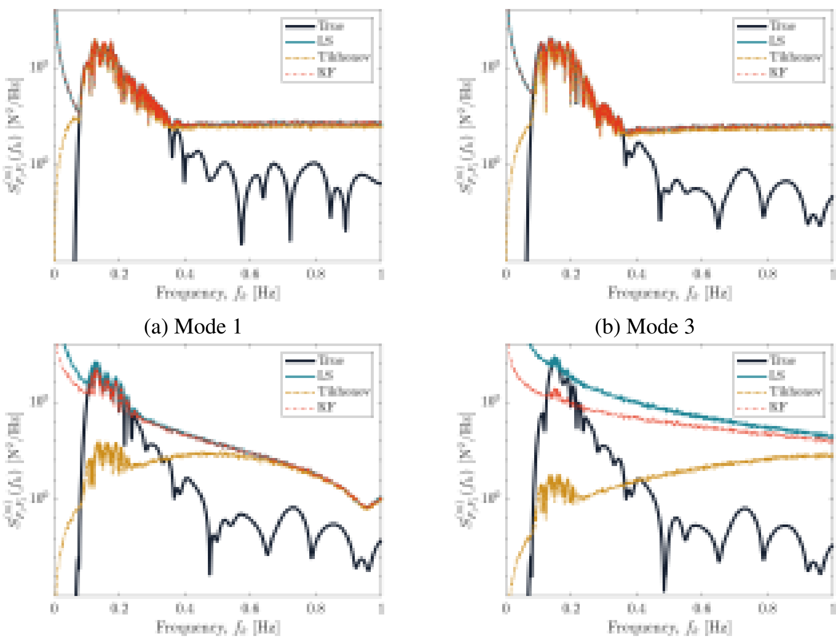

(a) Mode 1
(b) Mode 3
(c) Mode 5
(d) Mode 7

Figure 5: Power spectral density (PSD) of the estimated modal excitation forces for modes 1,3,5, and 7 compared with the true PSD, shown as a function of frequency.

5. Conclusions

This paper examined frequency- and time-domain inverse wave force estimation methods within a consistent hydroelastic modelling framework, focusing on the role of regularisation in stabilising the inverse problem. Three formulations were considered: unregularised frequency-domain least-squares (LS) inversion, Tikhonov-regularised frequency-domain inversion, and a time-domain joint input–state Kalman filter (KF).

Accurate reconstruction of excitation forces is primarily achieved in frequency regions where the hydroelastic forward operator is well conditioned, typically near modal resonances and for lower-order modes. In this regime, all estimators exhibit comparable performance, whereas away from resonance the LS solution shows strong variance amplification due to ill-conditioning.

Tikhonov regularisation stabilises the inversion and yields the lowest estimator variance, but introduces estimation bias by suppressing weakly observable force components. For higher-order modes this leads to underestimation of force energy and reduced reconstructed PSD, demonstrating that strong explicit regularisation may suppress physically relevant excitation content.

The time-domain Kalman filter provides a more balanced trade-off between variance reduction and bias through implicit regularisation introduced by the system dynamics. Although its variance is generally higher than that of the Tikhonov estimator, the reconstructed force spectra retain more physically relevant energy.

Overall, the results indicate that the primary limitation in inverse wave force estimation is governed by the sensitivity of the measured structural responses to the excitation forces, rather than by the specific estimation algorithm itself. In particular, poorly observable modal components and ill-conditioned frequency regions lead to strong noise amplification and increased estimation uncertainty. Explicit regularisation improves numerical stability but must be applied carefully to avoid excessive bias, while time-domain formulations benefit from incorporating temporal dynamics that naturally constrain the solution.

References

[1] U. Lajic Z. Jensen J.J. Nielsen, "Towards fault-tolerant decision support systems for ship operator guidance," *Reliability Engineering System Safety*, vol. 104, pp. 1–14, 2024.

[2] U. D. Nielsen, H. B. Bingham, A. H. Brodtkorb, T. Iseki, J. J. Jensen, M. Mittendorf, R. E. G. Mounet, Y. Shao, G. Storhaug, A. J. Sørensen, and T. Takami, "Estimating waves via measured ship responses," *Scientific Reports*, vol. 13, p. 17342, Oct. 2023. Publisher: Nature Publishing Group.

[3] Y.-S. Wu and W.-C. Cui, "Advances in the three-dimensional hydroelasticity of ships," *Proceedings of the Institution of Mechanical Engineers, Part M: Journal of Engineering for the Maritime Environment*, vol. 223, pp. 331–348, Sept. 2009.

[4] R. Taghipour, T. Perez, and T. Moan, "Hybrid frequency–time domain models for dynamic response analysis of marine structures," *Ocean Engineering*, vol. 35, pp. 685–705, May 2008.

[5] C. Van Zijl, J. Jovanova, and A. Grammatikopoulos, "Quantification of errors in frequency-domain inverse force estimation due to measurement noise," in *Proceedings of the Eleventh International Operational Modal Analysis Conference (IOMAC)*, 2025.

[6] W. Petersen, O. Øiseth, and E. Lourens, "Full-scale identification of the wave forces exerted on a floating bridge using inverse methods and directional wave spectrum estimation," *Mechanical Systems and Signal Processing*, vol. 120, pp. 708–726, Apr. 2019.

[7] Hansen, Per Christian, "Analysis of Discrete Ill-Posed Problems by Means of the L-Curve," *SIAM Review*, vol. 34, no. 4, pp. 561–580, 1992. _eprint: https://doi.org/10.1137/1034115.

[8] S. Gillijns and B. De Moor, "Unbiased minimum-variance input and state estimation for linear discrete-time systems with direct feedthrough," *Automatica*, vol. 43, pp. 934–937, May 2007.

[9] M. Ancellin and F. Dias, "Capytaine: a Python-based linear potential flow solver," *Journal of Open Source Software*, vol. 4, p. 1341, Apr. 2019.

[10] B.Gustavsen and A. Semlyen, "Rational approximation of frequency domain responses by vector fitting," *IEEE Trans. Power Delivery*, vol. 14, no. 3, pp. 1051–1061, 1999.

[11] D. E. Hasselmann, M. Dunckel, and J. A. Ewing, "Directional Wave Spectra Observed during JONSWAP 1973," *Journal of Physical Oceanography*, vol. 10, no. 8, pp. 1264 – 1280, 1980. Place: Boston MA, USA Publisher: American Meteorological Society.